Biophysical *Journal*
Article

Biophysical Society

Biophysical properties of tear film lipid layer II. Polymorphism of FAHFA

Xiaojie Xu,[1] Christopher Kang,[2] Rui Sun,[2] and Yi Y. Zuo[1,3,*]
[1]Department of Mechanical Engineering, University of Hawaii at Manoa, Honolulu, Hawaii; [2]Department of Chemistry, University of Hawaii at Manoa, Honolulu, Hawaii; and [3]Department of Pediatrics, John A. Burns School of Medicine, University of Hawaii, Honolulu, Hawaii

ABSTRACT Fatty acid esters of hydroxy fatty acids (FAHFAs) are a newly discovered class of endogenous lipids that consist of two acyl chains connected through a single ester bond. Being a unique species of FAHFAs, (O-acyl)-ω-hydroxy fatty acids (OAHFAs) differ from other FAHFAs in that their hydroxy fatty acid backbones are ultralong and their hydroxy esterification is believed to be solely at the terminal (ω-) position. Only in recent years with technological advances in lipidomics have OAHFAs been identified as an important component of the tear film lipid layer (TFLL). It was found that OAHFAs account for approximately 4 mol% of the total lipids and 20 mol% of the polar lipids in the TFLL. However, their biophysical function and contribution to the TFLL is still poorly understood. Here we studied the molecular biophysical mechanisms of OAHFAs using palmitic-acid-9-hydroxy-stearic-acid (PAHSA) as a model. PAHSA and OAHFAs share key structural similarities that could result in comparable biophysical properties and molecular mechanisms. With combined biophysical experiments, atomic force microscopy observations, and all-atom molecular dynamics simulations, we found that the biophysical properties of a dynamic PAHSA monolayer under physiologically relevant conditions depend on a balance between kinetics and thermal relaxation. PAHSA molecules at the air-water surface demonstrate unique polymorphic behaviors, which can be explained by configurational transitions of the molecules under various lateral pressures. These findings could have novel implications in understanding biophysical functions that FAHFAs, in general, or OAHFAs, specifically, play in the TFLL.

SIGNIFICANCE Recent lipidomic advances have led to the discovery of a unique species of fatty acid esters of hydroxy fatty acids, i.e., (O-acyl)-ω-hydroxy fatty acids, in the tear film lipid layer. However, the biophysical function of these lipids and their contribution to the tear film lipid layer are still poorly understood. Here we studied the molecular biophysical mechanisms of (O-acyl)-ω-hydroxy fatty acids using palmitic-acid-9-hydroxy-stearic-acid (PAHSA) as a model. With combined biophysical and atomic force microscopy experiments, we have explored the unique lipid polymorphism and collapse mechanisms of the PAHSA monolayer under various kinetic and temperature conditions. All-atom molecular dynamics simulations have revealed the molecular mechanisms of PAHSA polymorphism under lateral compression.

INTRODUCTION

Fatty acid esters of hydroxy fatty acids (FAHFAs) are molecules that contain a hydroxy fatty acid esterified by a fatty acid (1). Being a newly discovered class of endogenous lipids with potent antidiabetic and antiinflammatory activities (2,3), FAHFAs exist in an extremely low abundance in natural sources, including humans, animals, plants, and foods (4–6). Being a unique species of FAHFAs, (O-acyl)-ω-hydroxy fatty acids (OAHFAs) differ from other FAHFAs in that their hydroxy fatty acid backbones are ultralong, typically around 26–34 carbons in length, and their hydroxy esterification is believed to be solely at the terminal (ω-) position (7).

Only in recent years with technological advances in lipidomics have OAHFAs been identified as an important component of the meibomian lipids (8–12). Being the only polar lipid class other than phospholipids in the tear film lipid layer (TFLL), OAHFAs account for approximately 4 mol% of the total lipids and 20 mol% of the polar lipids (10,12). OAHFAs appear to play a significant physiological and biophysical role in eye health since it is the only class of lipids found to decrease in dry eye (13,14). Direct contribution of OAHFA deficiency to dry eye disease was recently established with *Cyp4f39*-knockout mice that

---

Submitted August 14, 2021, and accepted for publication December 22, 2021.

*Correspondence: yzuo@hawaii.edu

Editor: John Conboy.
https://doi.org/10.1016/j.bpj.2021.12.034

exhibited damaged corneal epithelium and shortening of tear film break-up time (15). The latest human study suggested that OAHFAs might be used as a biomarker for dry eye disease (16). However, compared to other lipids, biophysical study of OAHFAs is still scarce, likely in part due to technical difficulties in purifying large quantities of these lipids from complex meibomian gland secretions. The biophysical function of OAHFAs and their contribution to the TFLL are still poorly understood (15,17,18).

In a companion paper, we have studied the composition-function correlations of a recombinant artificial TFLL, under physiologically relevant conditions (19). Our artificial TFLL was composed of 40% behenyl oleate and 40% cholesteryl oleate that represent two nonpolar lipid classes, i.e., wax ester and cholesteryl ester in the natural TFLL, and 15% phosphatidylcholine and 5% palmitic-acid-9-hydroxy-stearic-acid (PAHSA) that represent the two predominant polar lipid classes in the natural TFLL (20). It should be noted that human meibomian lipids are composed of a complex mixture of different lipid classes, and each lipid class consists of numerous homologous lipid species varying in lengths, degrees of unsaturation, and branching (10,18,20). The major wax esters and cholesteryl esters found in human meibum are much longer than behenyl oleate and cholesteryl oleate used in our artificial TFLL (11,21,22). Moreover, PAHSA used in our artificial TFLL is only a remote model of OAHFAs. Due to its function in metabolic regulation and potential in glucose control, PAHSA has become the most extensively studied FAHFA (1,23), and it is readily available from commercial sources. We used PAHSA as an analog of OAHFAs to study the biophysics of TFLL since they share critical structural similarity that predominates their surface activities. Namely, both PAHSA and OAHFAs maintain their amphiphilicity through two hydrophilic moieties favoring contact with water, i.e., a relatively strong contact point through the negatively charged carboxyl group and a relatively weak contact point via the polar ester group. On the other hand, it is also important to understand the structural differences between these two FAHFAs. First, the hydroxy fatty acid backbone of PAHSA (C18) is much shorter than that of OAHFAs (C26–34). Second, PAHSA lacks the acyl chain unsaturation in OAHFAs since oleic acid (C18:1) has been identified as the most abundant acyl chain in OAHFAs (17). Third, with the ester group located at either the 9- or 5-position, PAHSA has a branched structure, whereas OAHFA should have a linear structure since its ester group is located at the ω-position (1).

In line with findings by other workers (24,25), our biophysical study suggested that the primary function of FAHFAs in the TFLL is not to reduce the surface tension (19). Rather, our study suggested that the main biophysical function of FAHFAs is to optimize the rheological properties of the TFLL (19). To further scrutinize the molecular mechanism by which the FAHFAs regulate and optimize the biophysical function of the TFLL, here we studied the detailed phase behavior of PAHSA molecules at the air-water surface, using combined in vitro biophysical simulations with constrained drop surfactometry (CDS), direct film imaging with atomic force microscopy (AFM), and in silico all-atom molecular dynamics (MD) simulations. We found that the biophysical properties of a dynamic PAHSA monolayer under physiologically relevant conditions depend on a balance between kinetics and thermal relaxation. Owing to their unique molecular structures of dual hydrophilic moieties, PAHSA molecules at the air-water surface demonstrate unique polymorphic behaviors and various collapse mechanisms. These findings could have novel implications in understanding the biophysical functions that FAHFAs, in general, or OAHFAs, specifically, play in the TFLL.

MATERIALS AND METHODS

Materials

Palmitic-acid-9-hydroxy-stearic-acid (PAHSA, C:18:0-C16:0) was purchased from Sigma-Aldrich and used without further purification. PAHSA was dissolved in chloroform as 1 mM stock solutions. Water used was Milli-Q ultrapure water with a resistivity greater than 18 MΩ•cm at room temperature.

Constrained drop surfactometry

CDS is a new-generation of droplet-based surface tensiometry technique developed in our laboratory (26). Detailed description of CDS can be found in the companion paper (19). Briefly, a trace amount of PAHSA was spread onto the air-water surface of a 10-μL droplet. The spread film was left undisturbed for 1 min to allow evaporation of solvent. The droplet was then slowly expanded to decrease the surface pressure to around zero (i.e., increasing the surface tension to around 70 mN/m). Subsequently, the spread lipid film was compressed at two extreme rates, i.e., 0.15 and 15 relative area per second (A%/s), and at two different environmental temperatures, i.e., 20°C and 34°C, with the latter representing the physiologically relevant temperature of the ocular surface. The low compression rate of 0.15 A%/s was used in our experiments to represents a quasi-static process, whereas the high compression rate of 15 A%/s was used to introduce sufficient kinematic effects into the study of the TFLL.

Atomic force microscopy

Lateral structure and topography of the PAHSA film were studied with the combination of in situ Langmuir-Blodgett (LB) transfer from the CDS and AFM (27). The lipid film was first LB transferred from the droplet by lifting a small piece of freshly peeled mica sheet at a speed of 1 mm/min. During the LB transfer process, the surface pressure of the lipid film was maintained at a constant value using closed-loop axisymmetric drop shape analysis (CL-ADSA) (28). Topographical images of the lipid film were obtained with an Innova AFM (Bruker, Santa Barbara, CA). Samples were scanned in air in contact mode using a silicon nitride cantilever with a spring constant of 0.12 N/m and a tip radius of 2 nm. Relative height differences between domains were determined with bearing analysis using Nanoscope Analysis (version 1.5).

Molecular dynamics simulations

All-atom MD simulations were performed to study the molecular organization of PAHSA molecules at the air-water surface. The force field parameterization of PAHSA was carried out using existing molecules in the CHARMM lipid force field (29). The detailed force field parameters are provided in the Supporting Material. The simulation box contained two symmetric PAHSA monolayers separated by a layer of TIP3 water of at least 4 nm thick. Periodic boundary conditions were enforced in all three directions. The system was generated using the PACKMOL software (30,31) and contained a total of 162 PAHSA molecules, i.e., 81 PAHSA per monolayer, 6186 TIP3 water molecules, and 17 ions of both Na^+ and Cl^- that mimic the physiological ionic concentration of 0.15 M. An illustration of the MD simulation system is depicted in Fig. 3 *a*. Steepest descent energy minimization was carried out, followed by 100 ns of equilibration. The axial, i.e., direction perpendicular to the monolayer, dimension of the system was ~25 nm after equilibrium, and the lateral dimension of the system was controlled at 5.2 nm × 5.2 nm, 6.2 nm × 6.2 nm, and 7.2 nm × 7.2 nm. The large axial dimension eliminates any possible interaction between the two PAHSA monolayers across the periodic boundaries. By varying the lateral dimension of the simulation box, the average area per lipid molecule and the corresponding surface tension were systematically controlled (32–35). Systems of each lateral dimension were simulated for 400 ns after the equilibrium. All simulations were conducted under NVT conditions and at a constant temperature of 34°C using the Nose-Hoover thermostat (36) in the GROMACS 2020.4 software package (37).

RESULTS

Compression isotherms of the PAHSA film

Fig. 1 shows the compression isotherms of the PAHSA monolayer at different temperatures (20°C and 34°C) and compression rates (0.15 and 15 A%/s), respectively. It is found that the compression isotherms of the PAHSA monolayer, at different temperatures and compression rates, are largely superimposed at the surface pressure lower than 25 mN/m. However, the collapse pressure (π_c) of the PAHSA monolayer differs under various experimental conditions. At 20°C and slow compression, the PAHSA monolayer collapses at 25 mN/m. Increasing temperature to 34°C, while maintaining the low compression rate, increases the π_c to 38 mN/m. The π_c of the PAHSA monolayer compressed at a high rate is found to be below 30 mN/m, at both 20°C and 34°C.

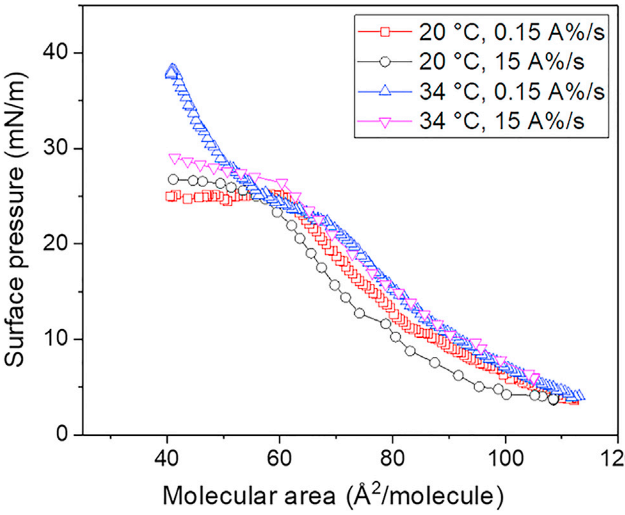

FIGURE 1 Compression isotherms of the PAHSA monolayer under four experimental conditions, i.e., 20°C and a low compression rate of 0.15 A %/s, 20°C and a high compression rate of 15 A%/s, 34°C and 0.15 A%/s, and 34°C and 15 A%/s.

It should be noted that these results are rather surprising since the experimental temperature of 34°C is very close to the melting temperature of PAHSA, i.e., 33.5°C. Hence, the PAHSA monolayer at 34°C is expected to be significantly more disordered than that at 20°C, whereas a lipid monolayer with a high fluidity usually instantaneously collapses upon quasi-static lateral compression without sustaining high surface pressures (38,39). However, here we found that the π_c of the PAHSA monolayer at 34°C, under quasi-static compression, is significantly higher than that at 20°C (38 versus 25 mN/m). A similar finding of the temperature dependence has been reported for the OAHFA monolayer (24), as will be discussed later.

Lateral structure and topography of the PAHSA film

Fig. 2 shows the lateral structure and topography of the PAHSA monolayer at three characteristic surface pressures, 10, 20, and 25 mN/m, respectively, at different temperatures (20°C and 34°C) and compression rates (0.15 and 15 A%/s), matching the experimental conditions used in Fig. 1. Reproducibility of the AFM experiments can be found in Fig. S1.

As shown in Fig. 2 *a*, at 20°C and slow compression, the PAHSA monolayer at 10 mN/m shows irregular flake-shaped domains about 1 nm higher than the surroundings. When the monolayer is compressed to 20 mN/m, these domains are further packed with relatively unchanged height differences. At 25 mN/m, i.e., the π_c under this experimental condition, the PAHSA monolayer collapses to form isolated multilayered collapse structures up to 14 nm higher than the surroundings.

In comparison, at 34°C and slow compression (Fig. 2 *c*), the PAHSA monolayer at 10 mN/m shows a network of ramified, fiber-like domains about 1 nm higher than the surroundings. When the monolayer is compressed to 20 mN/m, these higher domains form a denser network that covers most of the monolayer. At 25 mN/m, the fiber-like domains are compressed into larger pieces with a similar height as those at lower surface pressures, thus a large portion of the monolayer is covered with the higher domain. No collapse structure is found at 25 mN/m, which is consistent with the compression isotherm, i.e., π_c close to 38 mN/m under this experimental condition.

At 20°C and fast compression (Fig. 2 *b*), the PAHSA monolayer shows flake-shaped domains, similar to those shown in Fig. 2 *a*. However, in comparison to the slow compression shown in Fig. 2 *a*, all higher domains in Fig. 2 *b* are rapidly compacted into a fully packed monolayer without height contrasts at 20 mN/m. At 25 mN/m,

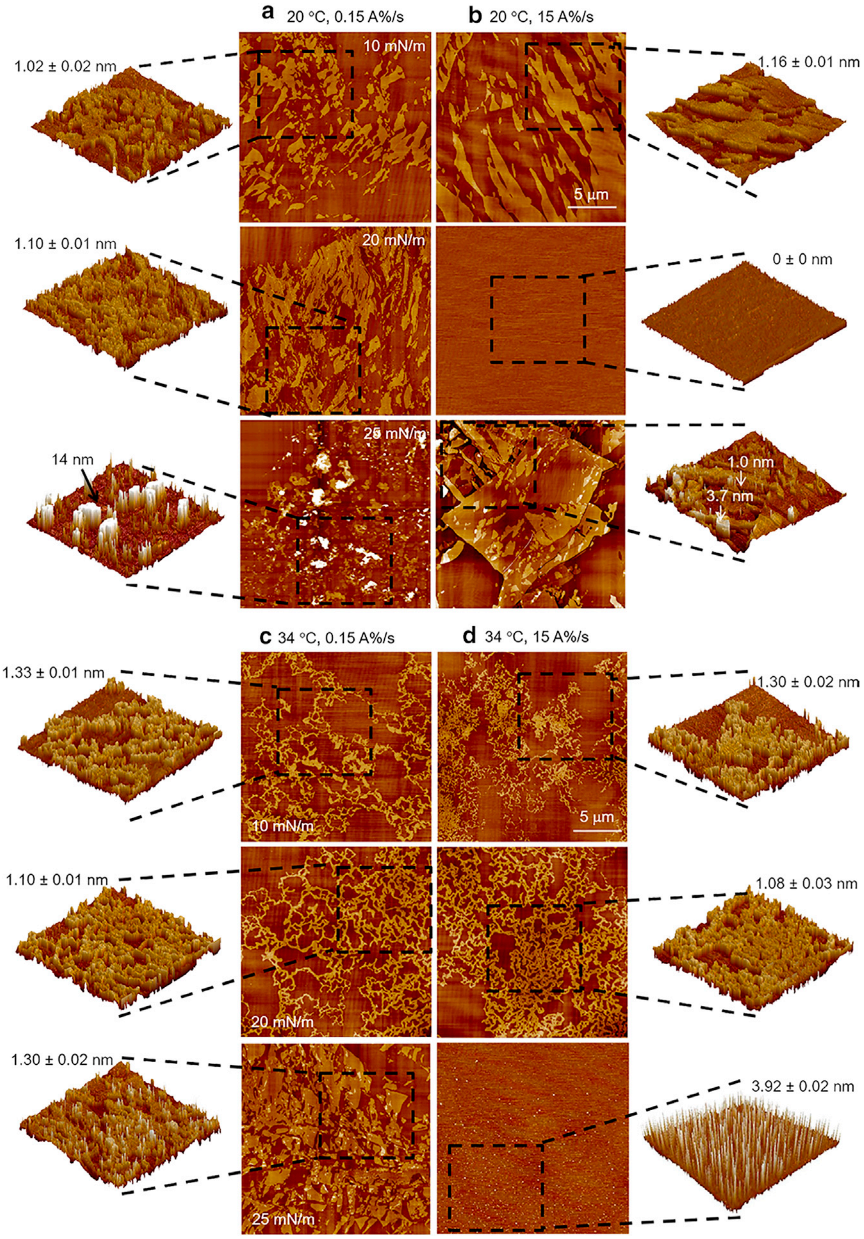

FIGURE 2 Lateral structure and topography of the PAHSA film at three characteristic surface pressures, i.e., 10, 20, and 25 mN/m, each under four experimental conditions. (*a*) 20°C and a low compression rate of 0.15 A%/s, (*b*) 20°C and a high compression rate of 15 A%/s, (*c*) 34°C and 0.15 A%/s, and (*d*) 34°C and 15 A%/s. All AFM images have the same scanning area of 20 μm × 20 μm and the same *z* range of 5 nm. Images in the first and last columns show the 3D rendering of the film indicated by black squares. The average height differences are shown as mean ± standard deviation. Arrows point to the height of specific features on the film. The bar represents 5 μm.

liquid-crystalline collapse, revealed as large-piece folding, initiates in the fully packed PAHSA monolayer, which is in contrast to the localized film collapse shown as individual protrusions at the same surface pressure shown in Fig. 2 *a*.

The domain structures at 34°C and fast compression (Fig. 2 *d*) are similar to those at 34°C and slow compression (Fig. 2 *c*). The PAHSA monolayer shows a network of ramified, fiber-like domains at 10 mN/m. These domains are compacted into a denser network at 20 mN/m, and then into a fully packed monolayer without height variations at 25 mN/m. At this surface pressure, numerous protrusions 4 nm higher than the compacted monolayer appear, indicating localized film collapse.

Molecular dynamics simulations of the PAHSA film

Fig. 3 shows the all-atom MD simulations of the PAHSA film at the air-water surface. Fig. 3 *a* shows the MD simulation model in which the two hydrophilic moieties of PAHSA are highlighted, with the more hydrophilic carboxyl group in blue and the less hydrophilic ester group in red. Fig. 3 *b* shows the density profiles of these two hydrophilic groups relative to the location of the air-water surface (defined by the density of water molecules). It can be seen that at a low surface pressure both the carboxyl group and the ester are solvated in water, with the carboxyl groups ~0.3 nm into the water while the esters reside at the

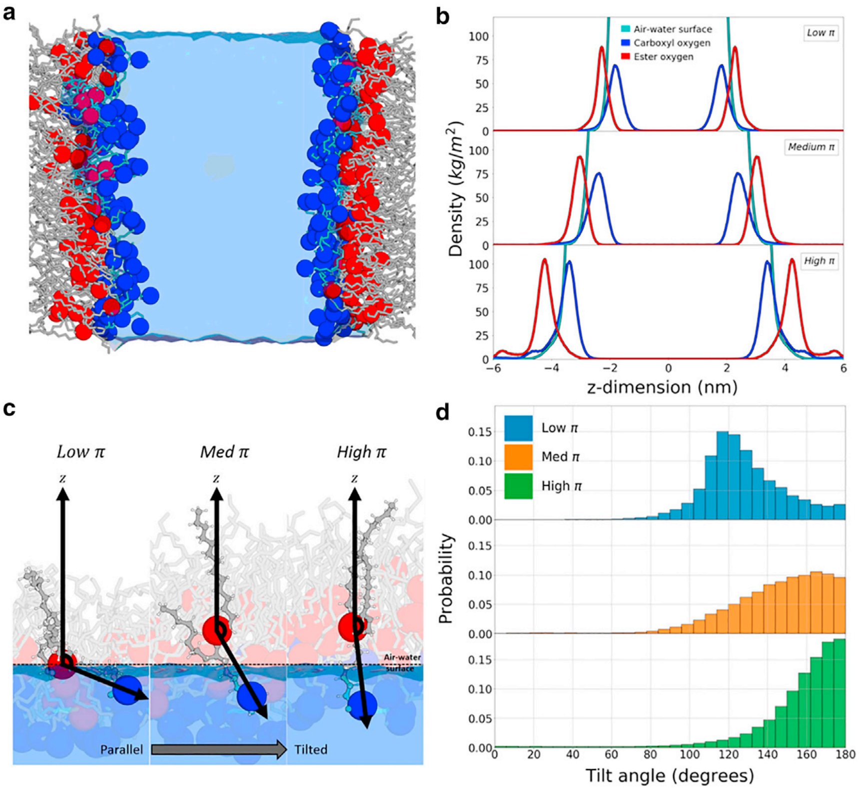

FIGURE 3 All-atom molecular dynamics simulations of the PAHSA monolayer at the air-water surface. (*a*) Demonstration of the simulation box. The carboxyl oxygen is represented by blue beads and the ester oxygen is represented by red beads. Hydrocarbon chains are represented by gray sticks. (*b*) Density profiles of the carboxyl group (in blue) and ester group (in red) of the PAHSA relative to the air-water surface (in light blue, measured by the density of water molecules) at increasing surface pressures. (*c*) Transition of the PAHSA molecule from a configuration "parallel" to the air-water surface, to a "tilted" configuration relative to the air-water surface, upon increasing surface pressure. The carbon atoms of the carboxyl oxygen are shown in blue, the ester oxygen is shown in red, and the rest of the carbon atoms are shown in gray. (*d*) Histograms of the average tilting angle of the vector connecting the carboxyl oxygen and the ester oxygen.

surface. When increasing surface pressure upon film compression, i.e., reducing the lateral dimension of the system, the esters are squeezed out of the bulk water. Fig. S2 shows the agreement between the MD-simulated compression isotherm and the experimentally determined compression isotherm at 34°C. Fig. 3 *c* is a cartoon representation of the molecular conformation of PAHSA at the air-water surface with increasing surface pressure. At a low surface pressure, the vector connecting the carboxyl and ester groups of the PAHSA molecule assumes a configuration parallel to the air-water surface, with both the carboxyl and ester groups lying inside water. With increasing surface pressure, the PAHSA molecule assumes a more and more tilted configuration, with the more hydrophilic carboxyl group remaining in water while the less hydrophilic ester is squeezed out. Fig. 3 *d* shows the quantified tilting angle measure at various surface pressures. It can be seen that the most probable tilting angle increases from approximately 120° to 180° with increasing surface pressure, indicating a transition of the PAHSA molecule from a parallel to a titled configuration (see an animation Video S1 of compressing a PAHSA monolayer in Supporting Material). This surface pressure-dependent change in the molecular tilting angle is consistent with the density profile (Fig. 3 *b*), collectively suggesting that the ester groups are squeezed out from the water as the surface pressure increases.

DISCUSSION

To date, most biophysical studies of artificial TFLL have ignored the effects of FAHFAs, in general, or OAHFAs, specifically. To the best of our knowledge, there are only a few available biophysical studies of OAHFAs in artificial TFLL (24,25,40,41). The OAHFAs used in all of these studies were synthetic and contained only short hydroxy fatty acid backbones up to 20 carbons. In the past two years, Paananen and co-workers have developed a series of synthetic, oleic acid (C18:1)-based OAHFAs with the hydroxy fatty acid backbone of various lengths, i.e., C12:0, C15:0, and C20:0 (25,40), and different chain saturation, e.g., C20:1 (41). They have studied extensively the biophysical properties of these synthetic OAHFAs using Langmuir trough. In general, they found that the π_c of OAHFAs at 35°C ranges from 35 mN/m for C20:1 (41) to 40 mN/m for OAHFAs with fully saturated backbones (25,40). These findings are in good agreement with the π_c of PAHSA found here at 34°C and slow compression (Fig. 1).

Butovich et al. first synthesized a model OAHFA, (O-oleyl)-ω-hydroxy palmitic acid (OOHPA), i.e., the C16:0-C18:1 OAHFA, in 2009 (11). Schuett and Millar have studied the surface activity of OOHPA (24). The compression isotherms obtained with OOHPA are in general agreement with those obtained here for PAHSA under slow compression (Fig. 1). Interestingly, they found that increasing temperature from 20°C to 35°C significantly increased the π_c of OOHPA from less than 10 to 45 mN/m. They were unable to explain this "unexpected" surface activity of OOHPA (24). A similar temperature dependence of the π_c is also found here with PAHSA (Fig. 1). We have further shown that with a high compression rate, the PAHSA film reaches the same π_c of 29 mN/m at both 20°C and 34°C. These results indicate that the biophysical properties of a dynamic PAHSA monolayer under physiologically relevant conditions must depend on a balance between kinetics (mostly controlled by the speed of film compression) and thermal relaxation (mostly controlled by temperature).

The different biophysical properties of the PAHSA monolayer under various temperatures and compression rates can be fully explained by the molecular organization and lateral structure of the monolayer revealed by AFM (Fig. 2). It is clear that the lateral domain structures of the PAHSA monolayer are predominantly affected by temperature, which determines the mobility and fluidity of the molecules, whereas the compression rate mostly affects the kinetic compactness of the monolayer. At 20°C, molecules in the PAHSA monolayer self-assemble into large flake-shaped crystalline domains. Such a loosely organized molecular structure can poorly absorb the kinetic energy of film compression, thus leading to film collapse at a low π_c (i.e., <30 mN/m). At 34°C, however, molecules in the PAHSA monolayer self-assemble into a more flexible and uniform, fiber-like network. Compared to the isolated flake-shaped domains formed at 20°C, this fiber-like network is more efficient in adsorbing the kinetic energy of film compression, especially at the low compression rate, thus maintaining a much higher π_c (i.e., 38 mN/m for slow compressions). It should be noted that this fiber-like network was also observed in the C20-OAHFA monolayer at 35°C using fluorescence microscopy (40), and in the human meibomian lipid film at 34°C and surface pressures lower than 10 mN/m using Brewster angle microscopy (42).

The unique phase behavior of PAHSA molecules at the air-water surface can be better understood with MD simulations (Fig. 3). It is well-known that both the time and length scales of all-atom MD simulations are too small to directly observe the phase behavior of biomembranes (43,44). However, all-atom MD simulations shed light on molecular orientation and rotation, which are of vital importance for understanding molecular mismatch and phase separation in lipid monolayers and membranes. A distinct difference in the molecular structure between phospholipids and PAHSA, as well as OAHFAs, is that instead of having only one hydrophilic headgroup as in phospholipids, PAHSA has two individual hydrophilic moieties, i.e., the more hydrophilic carboxyl group and the relatively less hydrophilic ester group. Both moieties are capable of interacting with water, albeit to different degrees. Consequently, the PAHSA monolayer at the air-water surface is expected to exhibit more complicated polymorphic behaviors than phospholipid monolayers. Our MD simulations have found that upon film compression, phase separations in the PAHSA monolayer are caused by a configurational transition from a parallel to a tilted configuration (Fig. 3 *c*). It is important to note that our MD simulations further show that the average distance between the carboxyl group and the ester group is ~1 nm (see Fig. S3). This distance is expected to be the mismatch in height between the parallel position and titled position of the PAHSA molecules, which is in good agreement with the height variations between phases determined with AFM (Fig. 2). The findings from our MD simulations are consistent with the molecular model of OAHFAs proposed by Butovich who predicted the amphiphilicity of these molecules from their unique chemical structures (18). In general, OAHFAs have two hydrophilic moieties, the strongly hydrophilic carboxyl headgroup, which is ionized at the physiological pH, and the mildly hydrophilic ester bond in the middle of the molecules since esters are capable of forming hydrogen bonds with water (18). The unique molecular structure of OAHFAs thus facilities

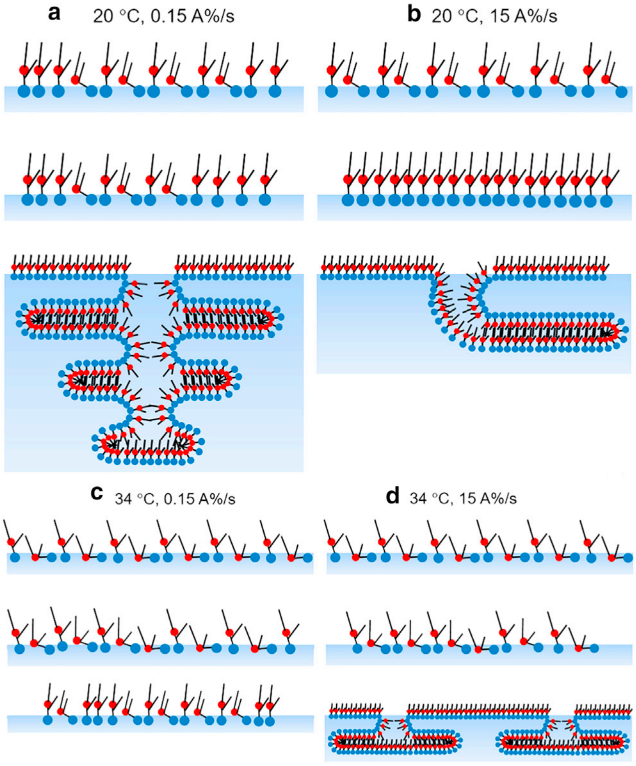

FIGURE 4 Cartoons of the compressed PAHSA monolayer at three characteristic surface pressures, i.e., 10, 20, and 25 mN/m, each under four experimental conditions. (*a*) 20°C and a low compression rate of 0.15 A %/s, where the PAHSA monolayer collapses as isolated large protrusions up to three bilayer stacks. (*b*) 20°C and a high compression rate of 15 A %/s, where the PAHSA monolayer collapses as large liquid-crystalline folds. (*c*) 34°C and 0.15 A%/s, where the PAHSA monolayer does not collapse at the surface pressure of 25 mN/m. (*d*) 34°C and 15 A%/s, where the PAHSA monolayer collapses as multiple, uniform-distributed, single bilayer budding. The carboxyl groups are represented by blue beads and the ester groups are represented by red beads.

their polymorphism at the air-water surface and their interactions with other polar and nonpolar lipids.

Taking together the results obtained from CDS, AFM, and MD simulations, Fig. 4 shows cartoons that describe the molecular organization of the PAHSA molecules at the air-water surface with increasing surface pressures of 10, 20, and 25 mN/m, under the four experimental conditions matching those studied in Figs. 1 and 2. Most importantly, Fig. 4 demonstrates the molecular mechanisms that are responsible for the collapse of the PAHSA monolayer under various kinetic and temperature conditions. At 20°C and slow compression (Fig. 4 *a*), the PAHSA monolayer collapses with isolated protrusions up to the thickness of three bilayer stacks (∼14 nm). At 20°C and fast compression (Fig. 4 *b*), the PAHSA monolayer collapses as large liquid-crystalline folds since the monolayer is kinetically fully packed before the folding. At 34°C and slow compression (Fig. 4 *c*), the PAHSA monolayer does not collapse at the surface pressure of 25 mN/m. At 34°C and fast compression (Fig. 4 *d*), the PAHSA monolayer collapses with multiple, uniform-distributed, small protrusions of only one bilayer in thickness (∼4 nm).

OAHFAs are the second most abundant amphiphilic lipid class found in meibum, accounting for ∼4 mol% of the total meibomian lipids (13,45). Hence, OAHFAs have been considered as a main surfactant in TFLL (13). However, our study showed that the primary biophysical function of OAHFAs may not be surface tension reduction but optimizing rheological properties of the TFLL (19). OAHFAs optimize the surface rheological properties of the TFLL by maintaining a highly elastic film across a range of oscillation frequencies (19). This finding is consistent with the clinical evidence that OAHFAs decrease with dry eye (14). Such compositional changes have been linked to the biophysical malfunction of increasing TFLL viscosity for patients with meibomian gland dysfunction (46–48). The optimal viscoelastic properties of OAHFAs are most likely related to their unique polymorphic behaviors at the air-water surface. Compared to phospholipid molecules, which have only one hydrophilic moiety, the dual hydrophilic groups of PAHSA molecules give them a new degree of rotational freedom when the lipid film is compressed. Consequently, the PAHSA monolayer may collapse with various molecular mechanisms (49,50), depending on the balance of kinetic compression and thermal relaxation.

CONCLUSIONS

Using combined biophysical experiments, AFM observations, and all-atom MD simulations, we have studied the detailed biophysical properties of FAHFAs using PAHSA as a model. It is concluded that the biophysical properties of a dynamic PAHSA monolayer under physiologically relevant conditions depend on a balance between kinetics (mostly controlled by the speed of film compression) and thermal relaxation (mostly controlled by temperature). We have revealed the unique lipid polymorphism and collapse mechanisms of the PAHSA monolayer at the air-water surface, under various kinetic and temperature conditions. Due to their structural similarities, the biophysical molecular mechanisms of PAHSA found here may be also applicable to OAHFAs. These findings could have novel implications in understanding biophysical functions that FAHFAs, in general, or OAHFAs, specifically, play in the TFLL.

SUPPORTING MATERIAL

Supporting Material can be found online at https://doi.org/10.1016/j.bpj.2021.12.034.

AUTHOR CONTRIBUTIONS

X.X. carried out the experiments and data analysis. C.K. carried out the molecular dynamics simulations and analysis. Y.Y.Z. designed the research and oversaw the experiments and analysis. Y.Y.Z, X.X., C.K., and R.S. wrote the paper. All authors discussed the results.

ACKNOWLEDGMENTS

This research was supported by the National Science Foundation grant number CBET-2011317 (to Y.Y.Z.) and the Mary & Paul Wagner Blindness Prevention Fund of the Hawaii Community Foundation grant number 20ADVC-102168 (to Y.Y.Z.). We thank the Information Technology Service (ITS) Cyberinfrastructure from the University of Hawai'i Manoa for the computational resources.

REFERENCES

1. Brejchova, K., L. Balas, …, O. Kuda. 2020. Understanding FAHFAs: from structure to metabolic regulation. *Prog. Lipid Res.* 79:101053.
2. Yore, M. M., I. Syed, …, B. B. Kahn. 2014. Discovery of a class of endogenous mammalian lipids with anti-diabetic and anti-inflammatory effects. *Cell.* 159:318–332.
3. Nelson, A. T., M. J. Kolar, …, D. Siegel. 2017. Stereochemistry of endogenous palmitic acid ester of 9-hydroxystearic acid and relevance of absolute configuration to regulation. *J. Am. Chem. Soc.* 139:4943–4947.
4. Kolar, M. J., A. T. Nelson, …, A. Saghatelian. 2018. Faster protocol for endogenous fatty acid esters of hydroxy fatty acid (FAHFA) measurements. *Anal. Chem.* 90:5358–5365.
5. Liberati-Čizmek, A.-M., M. Biluš, …, M. Cindrić. 2019. Analysis of fatty acid esters of hydroxyl fatty acid in selected plant food. *Plant Foods Hum. Nutr.* 74:235–240.
6. Zhu, Q. F., J. W. Yan, …, Y. Q. Feng. 2018. Comprehensive screening and identification of fatty acid esters of hydroxy fatty acids in plant tissues by chemical isotope labeling-assisted liquid chromatography-mass spectrometry. *Anal. Chem.* 90:10056–10063.
7. Hancock, S. E., R. Ailuri, …, S. J. Blanksby. 2018. Mass spectrometry-directed structure elucidation and total synthesis of ultra-long chain (O-acyl)-ω-hydroxy fatty acids. *J. Lipid Res.* 59:1510–1518.
8. Butovich, I. A. 2009. The Meibomian puzzle: combining pieces together. *Prog. Retin. Eye Res.* 28:483–498.
9. Chen, J., K. B. Green-Church, and K. K. Nichols. 2010. Shotgun lipidomic analysis of human meibomian gland secretions with

electrospray ionization tandem mass spectrometry. *Invest. Ophthalmol. Vis. Sci.* 51:6220–6231.

10. Butovich, I. A. 2011. Lipidomics of human Meibomian gland secretions: chemistry, biophysics, and physiological role of Meibomian lipids. *Prog. Lipid Res.* 50:278–301.
11. Butovich, I. A., J. C. Wojtowicz, and M. Molai. 2009. Human tear film and meibum. Very long chain wax esters and (O-acyl)-omega-hydroxy fatty acids of meibum. *J. Lipid Res.* 50:2471–2485.
12. Chen, J., K. K. Nichols, …, J. J. Nichols. 2019. Untargeted lipidomic analysis of human tears: a new approach for quantification of O-acyl-omega hydroxy fatty acids. *Ocul. Surf.* 17:347–355.
13. Willcox, M. D. P., P. Argueso, …, L. Jones. 2017. TFOS DEWS II tear film report. *Ocul. Surf.* 15:366–403.
14. Lam, S. M., L. Tong, …, M. R. Wenk. 2011. Meibum lipid composition in Asians with dry eye disease. *PLoS One.* 6:e24339.
15. Miyamoto, M., T. Sassa, …, A. Kihara. 2020. Lipid polarity gradient formed by ω-hydroxy lipids in tear film prevents dry eye disease. *eLife.* 9:e53582.
16. Khanal, S., Y. Bai, …, J. J. Nichols. 2021. Human meibum and tear film derived (O-acyl)-Omega-Hydroxy fatty acids as biomarkers of tear film dynamics in meibomian gland dysfunction and dry eye disease. *Invest. Ophthalmol. Vis. Sci.* 62:13.
17. Butovich, I. 2010. Biochemistry and biophysics of human and animal tear film lipid layer: from composition to structure to function. *Invest. Ophthalmol. Vis. Sci.* 51:4154.
18. Butovich, I. A. 2013. Tear film lipids. *Exp. Eye Res.* 117:4–27.
19. Xu, X., G. Li, and Y. Y. Zuo. 2021. Biophysical properties of tear film lipid layer I. Surface tension and surface rheology. *Biophys. J.*, Submitted as a companion paper.
20. Butovich, I. A., T. J. Millar, and B. M. Ham. 2008. Understanding and analyzing meibomian lipids–a review. *Curr. Eye Res.* 33:405–420.
21. Butovich, I. A., E. Uchiyama, and J. P. McCulley. 2007. Lipids of human meibum: mass-spectrometric analysis and structural elucidation. *J. Lipid Res.* 48:2220–2235.
22. Butovich, I. A. 2010. Fatty acid composition of cholesteryl esters of human meibomian gland secretions. *Steroids.* 75:726–733.
23. Zhou, P., A. Santoro, …, B. B. Kahn. 2019. PAHSAs enhance hepatic and systemic insulin sensitivity through direct and indirect mechanisms. *J. Clin. Invest.* 129:4138–4150.
24. Schuett, B. S., and T. J. Millar. 2013. An investigation of the likely role of (O-acyl) omega-hydroxy fatty acids in meibomian lipid films using (O-oleyl) omega-hydroxy palmitic acid as a model. *Exp. Eye Res.* 115:57–64.
25. Bland, H. C., J. A. Moilanen, …, R. O. Paananen. 2019. Investigating the role of specific tear film lipids connected to dry eye syndrome: a study on O-acyl-omega-hydroxy fatty acids and diesters. *Langmuir.* 35:3545–3552.
26. Valle, R. P., T. Wu, and Y. Y. Zuo. 2015. Biophysical influence of airborne carbon nanomaterials on natural pulmonary surfactant. *ACS Nano.* 9:5413–5421.
27. Xu, L., Y. Yang, and Y. Y. Zuo. 2020. Atomic force microscopy imaging of adsorbed pulmonary surfactant films. *Biophys. J.* 119:756–766.
28. Yu, K., J. Yang, and Y. Y. Zuo. 2016. Automated droplet manipulation using closed-loop axisymmetric drop shape analysis. *Langmuir.* 32:4820–4826.
29. Vanommeslaeghe, K., E. Hatcher, …, A. D. Mackerell, Jr. 2010. CHARMM general force field: a force field for drug-like molecules compatible with the CHARMM all-atom additive biological force fields. *J. Comput. Chem.* 31:671–690.
30. Martinez, L., R. Andrade, …, J. M. Martinez. 2009. PACKMOL: a package for building initial configurations for molecular dynamics simulations. *J. Comput. Chem.* 30:2157–2164.
31. Martínez, J. M., and L. Martínez. 2003. Packing optimization for automated generation of complex system's initial configurations for molecular dynamics and docking. *J. Comput. Chem.* 24:819–825.
32. Skibinsky, A., R. M. Venable, and R. W. Pastor. 2005. A molecular dynamics study of the response of lipid bilayers and monolayers to trehalose. *Biophys. J.* 89:4111–4121.
33. Baoukina, S., L. Monticelli, …, D. P. Tieleman. 2007. Pressure-area isotherm of a lipid monolayer from molecular dynamics simulations. *Langmuir.* 23:12617–12623.
34. Liu, B., M. I. Hoopes, and M. Karttunen. 2014. Molecular dynamics simulations of DPPC/CTAB monolayers at the air/water interface. *J. Phys. Chem. B.* 118:11723–11737.
35. Duncan, S. L., and R. G. Larson. 2008. Comparing experimental and simulated pressure-area isotherms for DPPC. *Biophys. J.* 94:2965–2986.
36. Nosé, S. 1984. A molecular dynamics method for simulations in the canonical ensemble. *Mol. Phys.* 52:255–268.
37. Abraham, M. J., T. Murtola, …, E. Lindahl. 2015. GROMACS: high performance molecular simulations through multi-level parallelism from laptops to supercomputers. *SoftwareX.* 1-2:19–25.
38. Smith, E. C., J. M. Crane, …, S. B. Hall. 2003. Metastability of a supercompressed fluid monolayer. *Biophys. J.* 85:3048–3057.
39. Yan, W., S. C. Biswas, …, S. B. Hall. 2007. The melting of pulmonary surfactant monolayers. *J. Appl. Physiol.* 102:1739–1745.
40. Paananen, R. O., T. Viitaja, …, L. Cwiklik. 2020. Interactions of polar lipids with cholesteryl ester multilayers elucidate tear film lipid layer structure. *Ocul. Surf.* 18:545–553.
41. Viitaja, T., J. E. Raitanen, …, F. S. Ekholm. 2021. The properties and role of O-acyl-ω-hydroxy fatty acids and type I-st and type II diesters in the tear film lipid layer revealed by a combined chemistry and biophysics approach. *J. Org. Chem.* 86:4965–4976.
42. Arciniega, J. C., E. Uchiyama, and I. A. Butovich. 2013. Disruption and destabilization of meibomian lipid films caused by increasing amounts of ceramides and cholesterol. *Invest. Ophthalmol. Vis. Sci.* 54:1352–1360.
43. Sodt, A. J., M. L. Sandar, …, E. Lyman. 2014. The molecular structure of the liquid-ordered phase of lipid bilayers. *J. Am. Chem. Soc.* 136:725–732.
44. Sodt, A. J., R. W. Pastor, and E. Lyman. 2015. Hexagonal substructure and hydrogen bonding in liquid-ordered phases containing palmitoyl sphingomyelin. *Biophys. J.* 109:948–955.
45. Brown, S. H., C. M. Kunnen, …, T. W. Mitchell. 2013. A comparison of patient matched meibum and tear lipidomes. *Invest. Ophthalmol. Vis. Sci.* 54:7417–7424.
46. Georgiev, G. A., P. Eftimov, and N. Yokoi. 2017. Structure-function relationship of tear film lipid layer: a contemporary perspective. *Exp. Eye Res.* 163:17–28.
47. Georgiev, G. A., N. Yokoi, …, R. Krastev. 2014. Surface relaxations as a tool to distinguish the dynamic interfacial properties of films formed by normal and diseased meibomian lipids. *Soft Matter.* 10:5579–5588.
48. Svitova, T. F., and M. C. Lin. 2013. Racial variations in interfacial behavior of lipids extracted from worn soft contact lenses. *Optom. Vis. Sci.* 90:1361–1369.
49. Baoukina, S., L. Monticelli, …, D. P. Tieleman. 2008. The molecular mechanism of lipid monolayer collapse. *Proc. Natl. Acad. Sci. U S A.* 105:10803–10808.
50. Lee, K. Y. C. 2008. Collapse mechanisms of Langmuir monolayers. *Annu. Rev. Phys. Chem.* 59:771–791.